ADVANCED MATERIALS INTERFACES
Open Access
www.advmatinterfaces.de

Texture-Enhanced Mechanical Stability of Transparent Electrodes for Flexible Optoelectronics with Near-Infrared Response

*Simon Rieckhoff, Florian Riesebeck, Marcos Soldera, Katja Mayer-Stillrich, Qiong Wang, Florian Ruske, Andrés Fabián Lasagni, and Christiane Becker**

Transparent electrodes with high conductivity and mechanical robustness are essential for flexible opto-electronic applications. Indium tin oxide (ITO) single layers have long been considered as unsuitable for flexible applications due to their brittleness. Here, it is shown that their mechanical stability can be substantially enhanced by texturing the flexible substrate. First, the opto-electronic performance of single ITO layers and ITO/Ag/ITO stacks on polyethylene terephthalate (PET) foils is evaluated numerically by means of Haacke's figure-of-merit. Single ITO layers are found to be the electrode of choice for applications with a near-infrared response due to their superior transparency. Following this, the sheet resistance of ITO layers is experimentally investigated on textured PET upon deformation parallel and perpendicular to a 1D texture grating. An "accordion-like" deformation perpendicular to the grating and high texture aspect ratios are shown to avoid crack formation and loss of conductivity in the ITO. Simulations prove the considerably reduced occurrence of mechanical stress in this case. It is further experimentally demonstrated that texturing foils increase transmittance and haze. The enhanced mechanical robustness and optical performance by using textured foils make single ITO layers promising candidates for flexible opto-electronic applications with a near-infrared response, such as all-perovskite tandem solar cells, thermal sensors, and photodetectors.

1. Introduction

Nowadays, transparent electrodes based on metal oxides, above all indium tin oxide (ITO), are the gold standard in opto-electronic devices on rigid substrates. These materials can simultaneously exhibit excellent transparency and conductivity and can be easily and homogeneously fabricated by means of magnetron sputtering on large areas on industrial scale. However, due to its brittleness, resulting in limited mechanical stability upon bending and the formation of cracks,[1,2] ITO layers are considered as non-ideal candidates for flexible opto-electronics. A second drawback of ITO is the scarcity of indium supply which led to considerable cost fluctuations in recent years. Alternative flexible transparent electrodes have been researched in the past years, such as ultra-thin metal films, metal nanowire networks, and metal meshes,[3] conductive polymers,[4] as well as carbon nanotubes and graphene.[5] All these approaches exhibit remarkable mechanical flexibility, but also their own problems to contend with. The challenges of thin metal films are island-like film growth if the targeted film is too thin or destructed transparency if too thick, or limited environmental stability against oxidation. The latter can be met by sandwiching the thin metal layer between two layers of metal oxides.[6] Nanowire networks often suffer from poor long-term stability due to deterioration of the wire-to-wire connection and weak adhesion. Metal meshes show the best balance between optical and electrical performance thanks to their highly tunable

---

S. Rieckhoff, F. Riesebeck, K. Mayer-Stillrich, Q. Wang, F. Ruske, C. Becker
Division Solar Energy
Helmholtz-Zentrum Berlin für Materialien und Energie GmbH Berlin
12489 Berlin, Germany
E-mail: christiane.becker@helmholtz-berlin.de

The ORCID identification number(s) for the author(s) of this article can be found under https://doi.org/10.1002/admi.202400922

DOI: 10.1002/admi.202400922

S. Rieckhoff
École Polytechnique Fédérale de Lausanne (EPFL)
Lausanne 1015, Switzerland

M. Soldera, A. F. Lasagni
Institut für Fertigungstechnik
Technische Universität Dresden
01062 Dresden, Germany

A. F. Lasagni
Fraunhofer–Institut für Werkstoff und Strahltechnik (IWS) Dresden
01277 Dresden, Germany

C. Becker
Hochschule für Technik und Wirtschaft Berlin
12459 Berlin, Germany

architecture. However, the fabrication of metal meshes is still costly and complicated. In contrast, conductive polymers such as poly(3,4-ethylenedioxythiophene) poly(styrenesulfonate) (PEDOT:PSS) can be fabricated at very low costs, but they struggle with low intrinsic conductivity, and poor environmental stability upon exposure to elevated temperatures, humidity, or UV irradiation. Tremendous progress has been made in emerging carbon nanomaterials research, however, a large-scale entry into the market is not foreseeable yet. It would be therefore highly desirable to find a transparent electrode that combines all the advantages of ITO with the additional advantage of increased tolerance to bending.

Here in this study, we aim at delivering some impulses to re-consider ITO as a transparent electrode for flexible opto-electronics by facing the challenge of brittleness. We begin with preliminary considerations on the requirements for transparent electrodes for opto-electronic applications with near-infrared response, such as all-perovskite tandem solar cells. After that, we investigate how the ITO sheet resistance evolves upon bending events if textured foils are used as flexible substrates. We use as flexible substrates polyethylene terephthalate (PET) foils with 1D texture grating fabricated with a two-step approach based on laser interference patterning of cylindrical molds followed by roll-to-roll hot embossing to transfer the microtextures to the PET foil. The resulting textured foils are covered with either bare ITO layers or InO / silver (Ag) / InO triple layers and their conductivity after bending is investigated, as well as their transparency. Depending on the bending direction – either parallel or perpendicular to the grating – and on the texture aspect ratio we find tremendously different sheet resistance evolutions. The experimental results are supported by mechanical finite element simulations reporting on texture-induced relaxation of layer stress.

2. Preliminary Considerations

We want to start the article with some considerations on transparent electrodes for opto-electronic applications with a near-infrared response, with a special view on all-perovskite tandem solar cells. Flexible perovskite solar cells are regarded as promising candidates for mobile energy systems, space energy systems, and portable functional devices due to high power-to-weight ratios.[7] Perovskite solar cells on flat flexible substrates coated with ITO have been reported,[8] however, a deterioration of the device performance was observed after bending, particularly for bending radii smaller than 10 mm.[9,10] Therefore, alternative transparent electrodes with higher bending durability are discussed in the context of perovskite solar cells, such as van der Waals epitaxy of ITO layers on mica substrate,[11] electrodes based on 2D materials,[12,13] and oxide/metal/oxide triple layers.[14] While the two formers have not entered the stage of large-scale fabrication yet, triple-layer electrodes might be an option for large-area flexible perovskite single-junction solar cells. Up to now, only a few flexible all-perovskite tandems have been reported.[15,16] Interestingly, when supporting the PET/ITO electrode with a molecule-bridged nickel oxide layer an improved bending durability was observed retaining the initial performance after ten thousand bending cycles with a bending radius of 15 mm.[16] Oxide/metal/oxide electrodes have not been reported yet in the context of all-perovskite tandem solar cells – for good reason as we see in the following:

Figure 1a shows the simulated optical transmittance of an ITO/Ag/ITO triple layer electrode on glass (see inset) for variable Ag layer thicknesses t_{Ag}. For the optical simulations we used the Matlab-based simulation software GenPro4,[17] which enables modeling solar cell stacks with ray tracing and the net-radiation method. The ITO layers are both 45 nm thick, hence, $t_{Ag} = 0$ nm corresponds to a 90 nm thin single ITO layer. An ITO/Ag/ITO triple-layer stack with $t_{Ag} = 8$ nm shows superior optical properties, i.e., a higher transmittance, compared to a single ITO layer for wavelengths shorter than ≈850 nm. However, for wavelengths longer than 850 nm (blue shaded area in Figure 1a the transmittance of the triple layer stack drops, and a single ITO layer performs better. Transparent electrodes are often characterized by the so-called Haacke figure-of-merit

$$FOM_{\text{Haacke}} = T^{10}/R_s \tag{1}$$

with T^{10} being the tenth power of the transmittance T, and R_s being the sheet resistance of the stack.[18] This figure-of-merit allows to evaluate the electrode with respect to transparency and conductivity. Depending on the spectral range of transmittance T, which is relevant for the targeted opto-electronic application, the shape of the curve changes. Figure 1b shows FOM_{Haake} of ITO/Ag/ITO triple-layer stacks calculated from the transmittance spectra as shown in Figure 1a. The white area indicates the practically relevant range of Ag layer thicknesses. Oh et al. found a remarkable mechanical robustness of ITO/Ag/ITO triple layer stacks with the Ag layer thickness ideally being in the range from 10–25 nm[6]: Thinning down the Ag film thickness further was found to increase transparency, but island-like film growth was found to sacrifice conductivity and mechanical robustness upon bending. Thicker Ag layers are found to deteriorate both, transparency and mechanical robustness. For the calculation of FOM_{Haacke} shown in Figure 1b the transmittance was averaged over three different ranges: The range 400 nm < λ < 800 nm is relevant for many types of single-junction solar cells, while the ranges 400 nm < λ < 1000 nm and 400 nm < λ < 1200 nm apply for multi-junction solar cells such as all-perovskite tandems. We used resistivity values of $\rho_{ITO} = 6.5 \times 10^{-4}$ Ωcm and $\rho_{Ag} = 7.8 \times 10^{-6}$ Ωcm extracted from experimentally measured sheet resistances on a single ITO layer (100 nm) and an ITO/Ag/ITO (45/12/45 nm) triple-layer electrode. The triple-layer sheet resistance R_s was regarded as the parallel of the three sheet resistances of the three layers:[19]

$$\frac{1}{R_s} = \frac{t_{ITO,1}}{\rho_{ITO,1}} + \frac{t_{Ag}}{\rho_{Ag}} + \frac{t_{ITO,2}}{\rho_{ITO,2}} \tag{2}$$

For single-junction perovskite solar cells the wavelength regime λ < 800 nm applies and ITO/Ag/ITO layer stacks clearly outperform a single ITO layer within the practical range of Ag layer thicknesses. However, considering the full range 400 nm < λ < 1200 nm as required, e.g., for all-perovskite tandem solar cells, the situation changes: There is only a very small Ag layer thickness range from ≈10 to 12 nm, and hence a very narrow processing window, where the oxide-metal-oxide electrode would outperform a single ITO layer with regard to transparency and

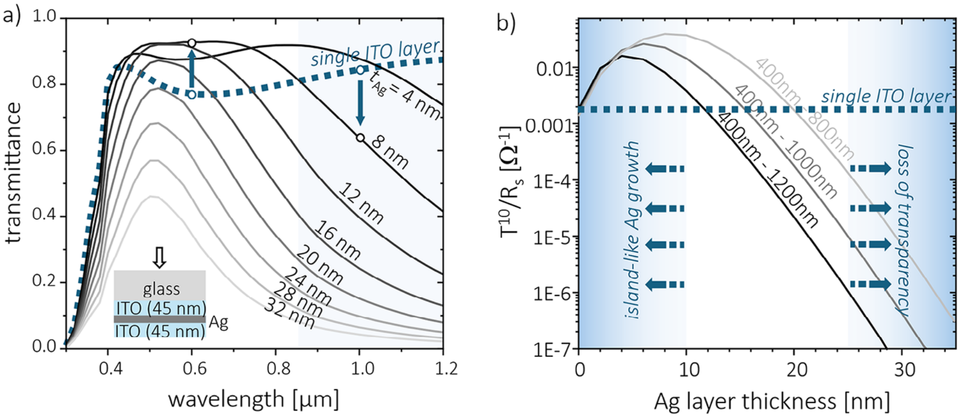

Figure 1. Single- versus triple-layer transparent electrodes. a) Simulated optical transmittance of an ITO/Ag/ITO triple-layer electrode on glass for variable Ag layer thicknesses t_{Ag} (as indicated). The ITO layers have a thickness of 45 nm each. The transmittance of a single ITO layer (t_{Ag} = 0 nm) is indicated as a blue dashed line. For wavelengths shorter than ≈850 nm, a triple layer stack with 8 nm Ag layer thickness clearly outperforms the single ITO layer; the opposite is the case for longer wavelengths (blue arrows). b) Haacke's figure of merit for the ITO/Ag/ITO triple-layer electrodes as a function of Ag layer thickness with the transmittance averaged for three different spectral ranges. The blue shaded areas indicate limited mechanical robustness of ITO/Ag/ITO triple layer electrodes according to ref.[6].

conductivity. For Ag layers thicker than that, the advantages of the single ITO-layer configuration outweigh the disadvantages, at least when considering sheet resistance and transparency only and disregarding mechanical stability aspects. If it would be possible to increase the tolerance of single ITO layers to mechanical bending, and if one would take into account that the production of a single-layer electrode is considerably less expensive and complicated than a triple triple layer oxide/metal/oxide stack, the single layer transparent oxides would be an attractive solution for opto-electronic applications with near-infrared response, such as all-perovskite tandem solar cells.

3. Results and Discussion

In this study, we investigate textured flexible substrates. Textures have been shown to exhibit an anti-reflective effect in perovskite solar cells.[20] In addition, it was shown that textured substrates can improve wettability and fabrication yield of solution-processed perovskite top cells in perovskite/silicon tandem solar cell devices.[21,22] Textured foil substrates might be therefore promising candidates for flexible perovskite-based solar cells enabling better film growth and higher efficiencies due to improved light management.

We used a two-step manufacturing process to pattern 200 µm thick PET foils with a periodic 1D grating with variable spatial periods and aspect ratios. Namely, a nickel cylindrical mold was first textured by direct laser interference patterning based on ps-laser source emitting IR (1064 nm) radiation. Thereafter, the patterned mold was mounted in a roll-to-roll system unit equipped with a hot embossing module, so that the PET foil was imprinted at 5 m/min. As example, **Figure 2** shows scanning electron microscopic (SEM) and confocal images of the resulting PET foils with (a,c,e) a spatial period of 1.4 µm and aspect ratio of 0.14, whereas similar images were taken for (b,d,f) a foil textured with a periodicity of 2.8 µm and aspect ratio of 0.22. The SEM images show well-defined line textures decorated by smaller quasi-periodic features (see labels in Figure 2). These sub-structures were transferred from the metal master and correspond to two types of laser-induced periodic surface structures (LIPSS): low spatial frequency LIPSS (LSFL) and high spatial frequency LIPSS (HSFL), as indicated in the figure. These self-assembled features appear inherently during the laser processing of metals upon using ultra-short laser pulses.[23] The fact that such nanostructures are visible in the PET foils is evidence that during the hot embossing step the soften polymer was able to fill completely the cavities of the stamp and replicated the texture with good fidelity. From the confocal images, an overall good texture uniformity can be observed, whereas the profiles allow for a better visualization of the grooves shape. The waviness present in the profiles can be regarded as an undesired consequence of using a laser beam with a Gaussian distribution of the intensity. Further analysis of similar structures using this method have been published elsewhere.[24]

Figure 3a depicts the layer stack configuration of the three flexible transparent electrodes investigated in this study. They consist either of a 100 nm thick magnetron sputtered ITO layer on flat (black frame) or on textured (colored frame) PET foil exhibiting a 1D grating texture with period *p*, texture height *h* and aspect ratio $AR = h/p$. As benchmark also a triple layer stack based on In_xO_y:Z (thereafter denoted as "InO") and silver (Ag) with the configuration InO (45 nm) / Ag (12 nm) / InO (45 nm) on flat PET foil (grey frame) is investigated. An oxide-Ag-oxide triple layer electrode with 12 nm thick Ag layer was chosen as benchmark for the following experimental investigations as it is in the optimum range enabling homogeneous, non-island-like Ag layer growth and still high transparency in the NIR optical regime (see Figure 1b). The samples underwent multiple bendings with bending radius 7 mm with deformation either parallel (Figure 3b) or perpendicular (Figure 3c) to the grating lines. In Figure 3d,e the corresponding sheet resistance R_s increasing factor of the different flexible transparent electrodes is shown as function of the number of bending cycles. In case of the single ITO layer on planar PET foil (black symbols), after 10 bending cycles the sheet resistance R_s increases from ≈30 $\Omega_\square$ to above 1300 $\Omega_\square$ (increasing factor >40). For more bendings the sheet

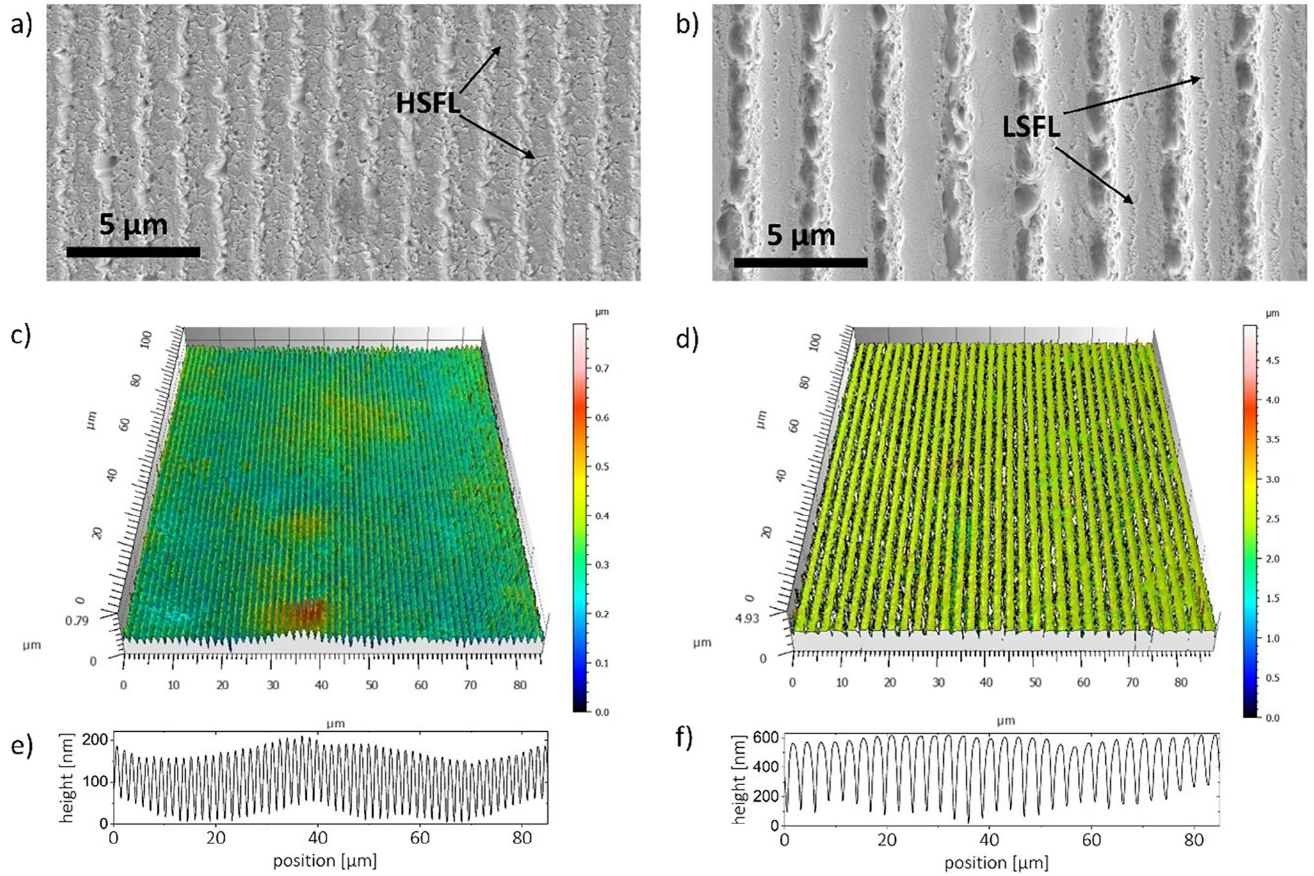

Figure 2. Structural properties of textured polyethylene terephthalate (PET) foils used in this study. a,b) Top view scanning electron microscopic image, c,d) confocal microscope image of the foil surface in 3D representation, and e,f) extracted profile perpendicular to the grating of foils featuring a spatial period of 1.4 µm and 2.8 µm, respectively.

resistance even shoots up beyond the 4-point-probe device measurement range (>2000 $\Omega_\square$). As expected, the InO/Ag/InO triple layer electrode withstands bending with a sheet resistance of ≈6 $\Omega_\square$ even not changing after 200 bending cycles, hence the increasing factor remains close to 1 (grey symbols).

In contrast, if the ITO layer is deposited on a textured PET foil exhibiting a 1D line grating, the resulting R_S is found to strongly depend on (1) the bending direction with respect to the grating and on (2) the *AR* of the line grating: In case of the deformation being parallel to the grating lines (colored, dashed lines in Figure 3d) R_s strongly increases upon bending. For very shallow textures ($AR = 0.04$ or 0.07) the dependence on bending resembles the behavior of the flat sample: after 20 bending cycles the sheet resistance has surpassed the measurement range of the 4-point-probe device. For texture *AR*s between 0.09 and 0.22 the R_s increasing factor quickly reaches a plateau value after ≈20 bendings in the range of 8 to 26, which does not substantially change up to 200 bending cycles. Interestingly, if the deformation is performed perpendicular to the grating (solid lines in Figure 3e), similar as with an accordion, one finds only a small increase of R_s for the textures with *AR*s larger than ≈0.1 (increasing factor 1.5–2). However, it seems that if the *AR* falls below a certain level, R_s strongly increases by a factor of ≈13 for $AR = 0.07$ and ≈45 for $AR = 0.04$. The fact that R_s reaches a plateau value after ≈20 bendings indicates that the detrimental effect of bending occurs within the first bending cycles. Interestingly, as no clear trend was observed for the different periods, the aspect ratio and texture orientation seem the dominant texture parameters that define the bending stability. The results are summarized in **Table 1**.

Figure 4 shows the cracking of the ITO layer after bending the foils with a bending radius of 7 mm. To make the cracks better visible, the samples were bent by fixing them on a curved sample holder with a curvature radius of 7 mm (Figure S1, Supporting Information). In the highest magnification, the grain structure of the room-temperature deposited ITO can be discerned revealing a grain size of ≈10 nm (Figure S2, Supporting Information). The deformation was either applied parallel (Figure 4a,b) or "accordion-like" perpendicular to the 1D grating (Figure 4c,d). The parallel bent sample shows a high density of visible cracks forming perpendicular to the 1D grating. We also carefully inspected the corresponding sample that was deformed perpendicular to the 1D grating ("accordion-like"). Cracks only occur sporadically here, e.g. in the upper part of Figure 4c. If so, they preferably occur in the texture valleys and their width is substantially smaller (Figure 4d) than in the parallel-bending case (Figure 4c). In the Supporting Information, we also present a collection of laser scanning microscopic images of samples after bending

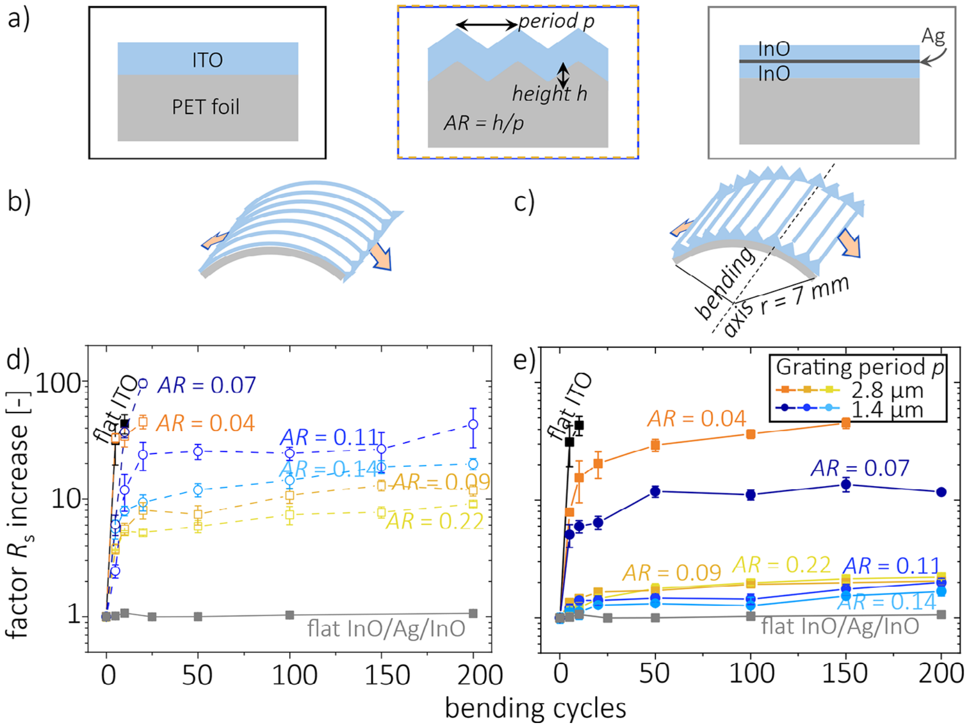

Figure 3. Mechanical stability of transparent electrodes on flat and textured PET foils after bending. a) Schematic illustration of the three flexible transparent electrodes under investigation, which are 100 nm ITO on flat (black frame) and textured (colored frame) PET foil, and an InO (45 nm)/Ag (12 nm)/InO (45 nm) triple layer stack (grey frame) on flat PET foil. During bending the textured samples are deformed either parallel (b) or perpendicular (c) to the grating lines. d) and e) Sheet resistance R_S increasing factor with respect to the non-bent case as a function of the number of bending cycles with a radius of 7 mm. The textured foils have a period of either 1.4 µm (blue-violet colors) or 2.8 µm (orange-yellow colors) with various texture heights leading to texture aspect ratios (*AR*) between 0.04 and 0.22 as indicated. Four-point-probe measurements were always performed parallel to the deformation.

parallel to the grating, with different texture periods and aspect ratios (Figure S3, Supporting Information). Here, cracks are only obvious in samples bent parallel to the grating and with *AR* smaller than 0.1. Summarizing, there are strong indications that the 1D grating texture can help to enhance the stability of ITO layers during bending, as long as the layer deformation takes place “accordion-like” perpendicular to the grating. These findings are in line with the sheet resistance results shown in Figure 3: A strong increase of R_s with a R_s plateau reached after few bending cycles can be ascribed to the crack formation in case of deformation parallel to the grating lines. In contrast, R_s remains at a relatively low level and only a few macroscopic cracks are observable for deformation “accordion-like” perpendicular to the grating.

To qualitatively investigate the effect of a 1D-textured PET substrate on the mechanical behavior of a 100 nm thin ITO film deposited atop, finite element simulations are performed using the ABAQUS software developed by Dassault Systems. Both materials are considered as homogeneous solids with 3D deformability. A simple static mechanical model is used assuming purely elastic behavior based on Young’s equation $\sigma = \varepsilon E$, with σ the stress, ε the strain (proportional deformation) and E Young’s modulus. For PET a density of $\rho_{PET} = 1.375$ g cm^{-3}, a Young’s modulus of $E_{PET} = 2.95$ GPa, and a Poisson ratio of $\nu_{PET} = 0.37$ are assumed.[25] The respective values for ITO are $\rho_{ITO} = 7$ g cm^{-3}, $E_{ITO} = 100$ GPa, and $\nu_{ITO} = 0.35$. The PET substrate and ITO layer are considered being assembled by a “Tie” interaction at their interface. Therefore, no movement or slipping between both materials is allowed.

We assume a triangular line grating with two different dimensions: one with 700 nm pitch and peak-to-valley height 260 nm,

Table 1. Sheet resistance R_s increasing factor of 100 nm thin ITO layers on 1D textured and planar PET foils compared to the initial value before bending after 150 bending cycles with bending radius 7 mm.

Texture properties			R_S [$\Omega_\square$] increasing factor after 150 bending cycles with deformation and measurement…	
aspect ratio	period [nm]	height [nm]	… ⊥ to grating (“accordion-like”)	…|| to grating
0 (flat)	–	–	>60 (not measurable)	
0.04	2800	100	45	>60 (not measurable)
0.07	1400	100	13	>60 (not measurable)
0.09–0.22	1400, 2800	150, 200	1.5 to 2	8 to 26

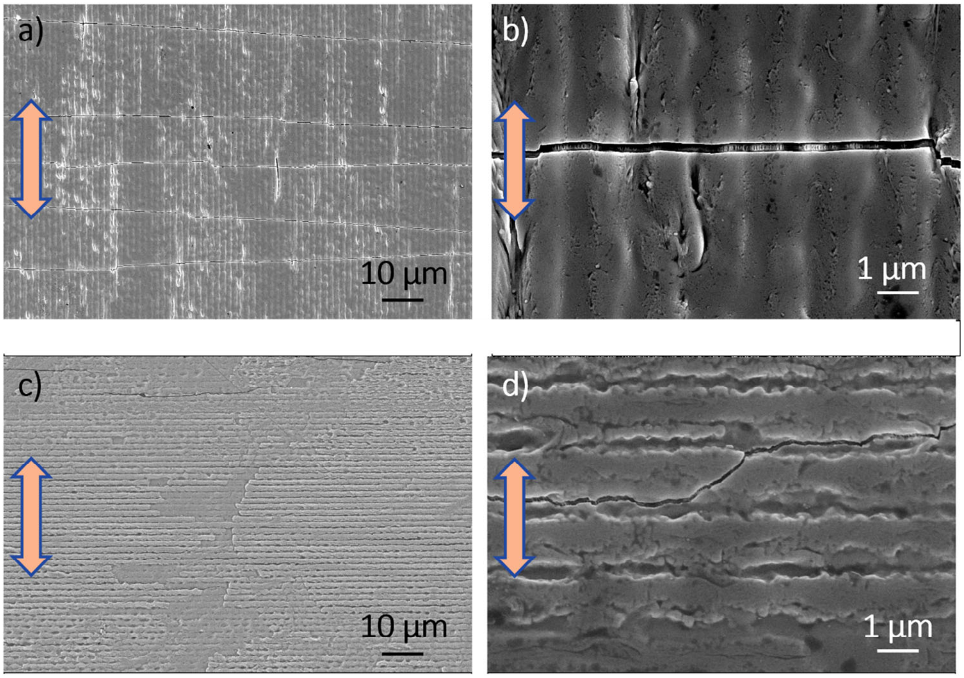

Figure 4. Scanning electron microscopic images of cracks in 100 nm thick ITO layers on textured (p = 1.4 µm, AR = 0.14) PET foils after 200 bendings with bending radius 7 mm with deformation parallel (a,b), and perpendicular (c,d) to the 1D grating as indicated by orange arrows. During imaging the samples were glued on a curved sample holder with a curvature radius 7 mm (see Figure S1, Supporting Information) such that cracks reopen und become more visible.

hence with an aspect ratio $AR = 0.37$ ("high AR"). The other one with pitch and height of 1520 and 280 nm, respectively, corresponding to $AR = 0.18$ ("low AR"), which is similar to the textures used in the bending experiments shown in Figure 3. As a reference, a planar configuration is modeled. Since the scale of grating textures and the thin film is very small compared to the size of the whole substrate, only a small volume of the top part of the PET-foil/ITO configuration is modeled comprising 4 texture periods, $2.8 \times 2.8 \times 2\ \mu m^{-3}$ and $6.08 \times 6.08 \times 5\ \mu m^{-3}$ for the $AR = 0.37$ and the $AR = 0.18$ texture, respectively.

In order to mimic the deformation that the defined geometry uptakes when the whole foil is bent, an external stress to one side surface is applied whereas the opposite side is pinned (see **Figure** 5a–c). For the simulation, the external stress is adapted such that the elongation remains in both materials the same. It is assumed that the small modeled top part deforms homogeneously over its thickness. Three different load cases are considered: Deformation of a fully planar configuration (Figure 5a), deformation parallel to the grating (Figure 5b), and deformation perpendicular to the grating (Figure 5c,d). In order to obtain the same deformation according to Young's equation, the applied stress on PET and ITO has to be adapted. In case of deformation perpendicular to the grating, the applied stress on PET and ITO are set to 100 MPa and 329 MPa, respectively for the $AR = 0.37$ grating. In case of deformation parallel to the grating and for the planar configuration the applied stress on PET and ITO are set to 100 MPa and 3390 MPa, respectively. The latter value is defined as the stress required to linearly deform the ITO in the same way as PET enduring 100 MPa. Figure 5a–d displays the stress distribution according to the Von Mises criterion. In the case of the deformation parallel to the grating (Figure 5b), the maximal stresses are relatively homogenously distributed over the ITO layer. In the case of bending perpendicular to the grating ("accordion-like"), the stress distribution is not homogeneous anymore: It reaches maximum stress in the texture valleys and lower stress values at the texture hills (Figure 5c,d). Figure 5e,f summarizes the maximal stress in the ITO layer for the three load cases (deformation perpendicular and parallel to the grating, as well as the planar configuration) and for the two different texture aspect ratios as a function of the elongation. A linear correlation between elongation and layer stress is observed. In the case of the "high AR" sample, stresses are almost an order of magnitude (factor 8.6) reduced for deformation perpendicular to the grating compared to both, the load case with deformation parallel to the grating and the flat case (Figure 5e). For the "low AR" sample, which is comparable to the samples experimentally investigated in this study, the stress is still relieved by a factor of 3.3 compared to the planar and parallel-to-the-grating-deformed sample. These findings can be correlated to the observed cracks shown in Figure 4. If bent parallel to the grating a high density of evenly distributed cracks is observed over the ITO surface. In the case of "accordion-like" bending perpendicular to the grating, however, the density and width of cracks are much lower. When the cracks appear, it is in the texture valleys, where the simulations predicted the highest stress values. Similar nanostructure-enhanced bending durability had been reported on amorphous silicon thin film solar cells on regular nanocone arrays on plastic substrates[26] and on perovskite solar cells on 3D nanopillar arrays.[27]

Figure 6 shows the transmittance (solid lines) and the haze (dashed lines) spectra of various flexible transparent electrodes.

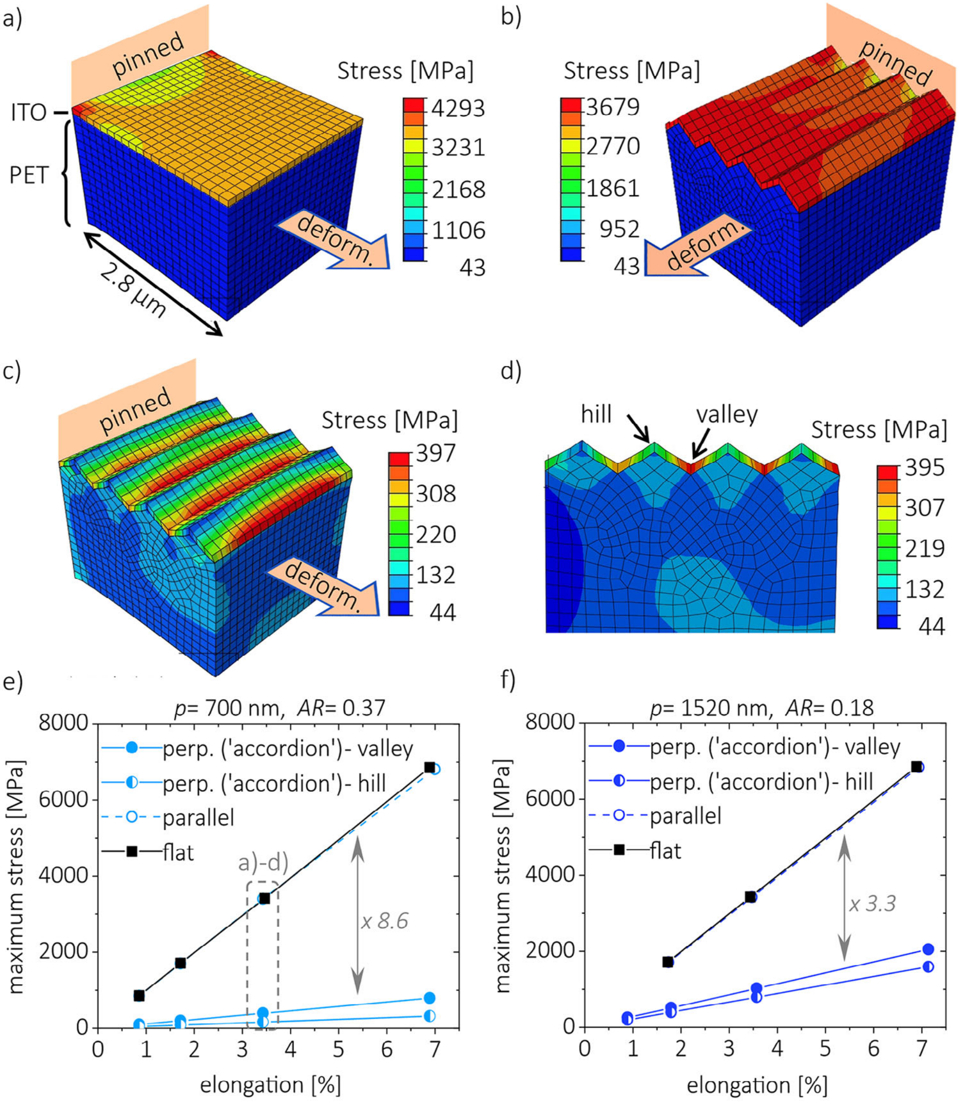

Figure 5. Stress-strain simulations of 100 nm thin ITO layers on flat (a) and 1D textured (b-d) PET substrates with deformation parallel (b) and perpendicular (c,d) to the line grating as indicated by orange arrows. The 1D gratings shown in a)-d) have a grating with 700 nm period and 260 nm height (aspect ratio $AR = 0.37$, "high *AR*") and an elongation by 3.5%. e) Maximum stress in the ITO layer versus elongation for different bending directions as indicated in the legend for a "high *AR*" sample and f) for a "low *AR*" sample with 1520 nm period and 280 nm height (aspect ratio $AR = 0.18$).

As expected from the optical simulations shown in Figure 1, the flat triple layer electrode outperforms the flat single ITO layers in the wavelength regime between 450 and 750 nm in terms of transmittance, but for longer wavelengths, the triple layer transmittance steeply decreases owing to the rise of reflectance. What is of interest now is the influence of the textures on the optical performance. For visible wavelengths, the textured ITO layers exhibit transmittance values close to their flat counterpart. However, for NIR wavelengths a clear anti-reflective effect can be observed by texturing increasing the transmittance by 5% absolute – an effect that is more pronounced the greater the *AR* is. A strong dependence on *AR* can also be observed for the diffuse transmittance. The sudden overall increase of transmittance at ≈720 nm for all ARs can be attributed to an abrupt decreased number of diffracted orders reflected back into the foil with 1.4 µm periodic grating, as similarly reported in reference.[28] This assumption is underlined by the fact that for the 2.8 µm periodic grating the respective transmittance increase is observed roughly at the double wavelength of 1400 nm (see Figure S4, Supporting Information). The findings are beneficial for solar cell applications as the increased total and diffuse transmittance allow for a better light in-coupling and enhancement of the light path in the solar cell absorber. The latter is particularly relevant for weakly absorbing materials such as crystalline silicon and narrow bandgap perovskites. The enhanced light transmittance in the long wavelength ranging from 720 nm to beyond 1250 nm featured in the textured ITO / PET electrodes is of particular interest for the NIR and IR response of optoelectronic devices. For instance, in the application of flexible tandem photovoltaics, such as all-perovskite or perovskite / CIGS tandems, light is split into two

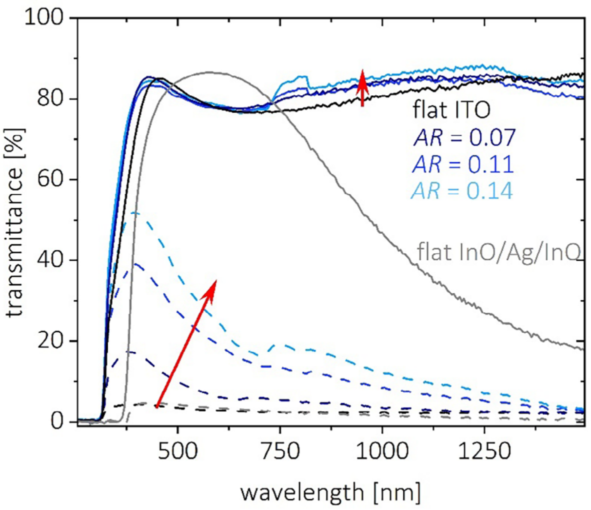

Figure 6. Optical properties. Total (solid lines) and diffuse transmittance (dashed lines) of 100 nm ITO on flat (black) and textured (bluish colors) PET foil, and an InO (45 nm) / Ag (12 nm) / InO (45 nm) triple layer stack (grey) on flat PET foil. The textured foils have a period of 1.4 µm and texture heights of 100 nm (*AR* = 0.07, dark blue), 150 nm (*AR* = 0.11, medium blue), and 200 nm (*AR* = 0.14, light blue). Red arrows indicate increasing *AR*s. The PET substrate foils of the single and triple-layer stacks had different margins explaining the different absorption onset in the UV.

parts where the short wavelength spectrum part is harvested by the perovskite top cell and the longer wavelength spectrum part (up to 1200 nm) reaches the bottom cell. By applying the textured electrodes studied in this work, an increase of light reaching the bottom cell is expected, enabling highly efficient tandem devices.

4. Conclusion

We fabricated flexible, transparent ITO electrodes deposited on textured PET foils with 1D line gratings fabricated by combining direct laser interference patterning and roll-to-roll hot embossing. The bending durability of these transparent electrodes was found to considerably improve compared to corresponding flat electrodes when deformation took place perpendicular to the line grating as in an accordion. Mechanical simulations proved that the enhanced bending durability arises from reduced stress in the ITO layer – an effect that increases with larger texture aspect ratios. Further, the transmittance of the electrodes was found to substantially increase in the near-infrared spectral range by texturing, as well as haze was found to increase by texturing. We benchmarked all results on textured PET/ITO electrodes by oxide/metal/oxide triple-layer electrodes. For opto-electronic applications in the visible regime, the triple-layer electrodes are found to outperform PET/ITO electrodes concerning both, bending durability and transparency. However, when considering a broader spectral range up to the near-infrared, the result turns around.

Summarizing, the results show that texturing foil substrates can kill two birds with one stone in the field of flexible photovoltaics: First, the texture increases transmittance and haze, and second, the texture can massively increase the mechanical stability of transparent ITO electrode films upon bending. Due to these two reasons and a remarkable transparency in the near-infrared region, ITO electrodes on textured plastic substrates are therefore an appealing option for flexible opto-electronic applications with near-infrared response, such as multi-junction solar cells, infrared cameras, thermal sensors and photodetectors.

5. Experimental Section

Fabrication—Textured Foils: The textured polyethylene terephthalate (PET-GAG) foils (Pütz Folien GmbH+Co. KG, Germany) were fabricated in a two-step process. First, a Ni sleeve (300 mm in length, 300 mm in diameter, and 200 µm thickness) was patterned by two-beam Direct Laser Interference Patterning (DLIP) using a self-developed setup (by Fraunhofer IWS – TU Dresden) equipped with a ps-pulsed solid-state laser (Edgewave PX200, Germany) with a nominal output power of 10 W. The laser source emitted radiation at a wavelength of 1064 nm with a pulse duration of 10 ps at a repetition rate of 10 kHz. The angle between the interfering beams was set to achieve a spatial period between the interference maxima of either 1.4 or 2.8 µm. The pulse-to-pulse overlap was set to 60, 80, and 95% in order to structure grooves with a targeted depth of 100, 150, and 200 nm, respectively, for the gratings with a spatial period of 1.4 µm, whereas overlaps of 60, 80, and 90% were applied for targeting structure heights of 100, 250, and 600 nm, respectively, for 2.8 µm periodic texture. The fluence per pulse on the sample was set to 0.36 and 0.52 J cm^{-2} for the periods of 1.4 and 2.8 µm, respectively. The hatch distance was set at 100 µm and the spot had a diameter of 190 µm. Subsequently, the laser-patterned sleeve was mounted in a roll-to-roll hot embossing system (R2R Basecoater BC51, Coatema Coating Machinery GmbH, Germany). The temperature of the top roller containing the DLIP-treated sleeve was held at 75 °C, slightly above the Vicat softening point of PET to avoid sticking to the structured sleeve, while the bottom counter-roller was kept at room temperature. The PET foil, with a nominal thickness of 200 µm, was embossed at a web speed of 5 m min^{-1}, which according to previous studies guarantees a good texture quality, uniformity and fidelity compared to the master texture.[24] The system pressure was 6 bar and the gap between the rollers was set at 185 µm, which is 15 µm lower than the foil thickness. Further details on the employed setups and manufacturing processes can be found elsewhere.[29]

Fabrication—ITO Single Layers: The single ITO layers were deposited at room temperature using a Roth&Rau magnetron sputtering tool with a DC power of 70 W at 0.6 µbar base pressure and 6 mbar working pressure. To ensure a layer thickness of 100 nm on all samples, the deposition time was adjusted to the different texture surface enhancement factors.

Fabrication—InO / Ag / InO Triple Layer Stacks: In_xO_y:Z/Ag/ In_xO_y:Z triple layers were done on an inline-like sputtering tool from Leybold Optics GmbH. The tool is called A600V7 and can do sputter depositions in DC and pulsed DC mode of planar and rotary targets with a length of 600 mm in vertical position. The In_xO_y:Z was done with 1.6% O_2 and 0.6% H_2 at a pulsed DC power of 4 kW and 5.5 µbar. The ultra-thin Ag layer in between was done with a DC power of 1 kW and 4 µbar. All layers were processed without vacuum break and non-heated.

Characterization—UV–vis: Transmittance and reflectance measurements were conducted with a UV/Vis/NIR spectrophotometer with an integrating sphere (Lambda 1050+, Perkin Elmer).

Characterization—Four-Point Probe: During the bending, the sheet resistance was measured using a handheld 4-point probe tool by Schuetz Messtechnik GmbH. According to the specifications, the tool has a maximum measuring range of up to 1000 $\Omega_{\square}$, but also values up to 2000 $\Omega\square$ were measured. Whenever the maximum measurable sheet resistance was reached, no more values could be measured, which led to some graphs ending after fewer bending cycles.

Characterization—Confocal Microscope: A VK-X260 (Keyence) confocal laser scanning microscope was used to show the condition of the ITO layer after bending. The objective lens system of the setup allows a range of 10× to 150× magnification and the practical resolution limit is ≈1 µm. For measuring the topography of the textured PET foils, a confocal microscope

(Sensofar S-Neox, Spain) was used employing a 150× magnification objective resulting in a lateral resolution of 140 nm and a vertical resolution of 1 nm.

Characterization—Scanning Electron Microscope: SEM images were taken using a Zeiss MERLIN field emission microscope with a Gemini 2 column. Presented images except image Figure 4c were acquired using the In-Lense detector. For Figure 4c the secondary electron (SE) detector was used.

Simulations—Optical Simulations: For the optical simulations the Matlab-based simulation software GenPro4,[17] was used, which enables modeling solar cell stacks with ray tracing and the net-radiation method. In the simulations, the thin ITO and Ag layers with thicknesses in the nanometer regime were treated as coherent "coatings" accounting for interference effects, while the several hundreds of micrometers thick PET foil was treated as incoherent "layer" not accounting for interference. The PET/ITO(/Ag/ITO) layer stacks were regarded as surrounded by infinite halfspaces of air.

Simulations—Mechanical Simulations: For mechanical simulations the finite element method software Abaqus, developed by Dassault Systems, was used. The material properties were taken from.[25] The PET substrate and ITO layer were considered being assembled by a "Tie" interaction at their interface. Therefore, no movement or slipping between both materials was allowed.

Supporting Information

Supporting Information is available from the Wiley Online Library or from the author.

Acknowledgements

This work was partly carried out in the framework of the Reinhart Koselleck project (323477257), which has received funding from the German Research Foundation (German: Deutsche Forschungsgemeinschaft DFG), and in the framework of the European project JUMP-INTO-SPACE, which has received funding from the European Innovation Council (EIC) under grant agreement No 101162377. F.Rie. gratefully acknowledges funding from the German Federal Ministry of Education and Research (BMBF) for the SolarTAP innovation platform under the Helmholtz Innovation Platforms funding line.

Conflict of Interest

The authors declare no conflict of interest.

Data Availability Statement

The data that support the findings of this study are available from the corresponding author upon reasonable request.

Keywords

all-perovskite tandem solar cells, bending, direct laser interference patterning, flexible transparent electrodes, texturing, transparency

Received: November 19, 2024
Revised: March 3, 2025

---

[1] V. Zardetto, T. M. Brown, A. Reale, A. Di Carlo, *J. Polym. Sci.* **2011**, *49*, 638.
[2] M. N. Saleh, G. Lubineau, *Sol. Energy Mater. Sol. Cells* **2014**, *130*, 199.
[3] X. Lu, Y. Zhang, Z. Zheng, *Adv. Electron. Mater.* **2021**, *7*, 2001121.
[4] S. Kirchmeyer, K. Reuter, *J. Mater. Chem.* **2005**, *15*, 2077.
[5] D. S. Hecht, L. Hu, G. Irvin, *Adv. Mater.* **2011**, *23*, 1482.
[6] S. J. Oh, S. Lee, K. C. Choi, J. H. Kwon, T.-S. Kim, *J. Mater. Chem. C* **2023**, *11*, 7262.
[7] Y. Gao, K. Huang, C. Long, Y. Ding, J. Chang, D. Zhang, L. Etgar, M. Liu, J. Zhang, J. Yang, *ACS Energy Lett.* **2022**, *7*, 1412.
[8] X. Wu, G. Xu, F. Yang, W. Chen, H. Yang, Y. Shen, Y. Wu, H. Chen, J. Xi, X. Tang, Q. Cheng, Y. Chen, X.-M. Ou, Y. Li, Y. Li, *ACS Energy Lett.* **2023**, *8*, 3750.
[9] M. Pandey, Z. Wang, G. Kapil, A. K. Baranwal, D. Hirotani, K. Hamada, S. Hayase, *Adv. Eng. Mater.* **2019**, *21*, 1900288.
[10] B. J. Kim, D. H. Kim, Y.-Y. Lee, H.-W. Shin, G. S. Han, J. S. Hong, K. Mahmood, T. K. Ahn, Y.-C. Joo, K. S. Hong, N.-G. Park, S. Lee, H. S. Jung, *Energy Environ. Sci.* **2015**, *8*, 916.
[11] C. Jia, X. Zhao, Y.-H. Lai, J. Zhao, P.-C. Wang, D.-S. Liou, P. Wang, Z. Liu, W. Zhang, W. Chen, Y.-H. Chu, J. Li, *Nano Energy* **2019**, *60*, 476.
[12] J. Yoon, H. Sung, G. Lee, W. Cho, N. Ahn, H. S. Jung, M. Choi, *Energy Environ. Sci.* **2017**, *10*, 337.
[13] X. Shen, X. Lin, Y. Peng, Y. Zhang, F. Long, Q. Han, Y. Wang, L. Han, *Nano-Micro Lett.* **2024**, *16*, 201.
[14] M. Girtan, B. Negulescu, *Opt. Mater.:X* **2022**, *13*, 100122.
[15] A. F. Palmstrom, G. E. Eperon, T. Leijtens, R. Prasanna, S. N. Habisreutinger, W. Nemeth, E. A. Gaulding, S. P. Dunfield, M. Reese, S. Nanayakkara, T. Moot, J. Werner, J. Liu, B. To, S. T. Christensen, M. D. McGehee, M. F. A. M. Van Hest, J. M. Luther, J. J. Berry, D. T. Moore, *Joule* **2019**, *3*, 2193.
[16] L. Li, Y. Wang, X. Wang, R. Lin, X. Luo, Z. Liu, K. Zhou, S. Xiong, Q. Bao, G. Chen, Y. Tian, Y. Deng, K. Xiao, J. Wu, M. I. Saidaminov, H. Lin, C.-Q. Ma, Z. Zhao, Y. Wu, L. Zhang, H. Tan, *Nat. Energy* **2022**, *7*, 708.
[17] R. Santbergen, T. Meguro, T. Suezaki, G. Koizumi, K. Yamamoto, M. Zeman, *IEEE J. Photovoltaics* **2017**, *7*, 919.
[18] G. Haacke, *J. Appl. Phys.* **1976**, *47*, 4086.
[19] G. Cesarini, G. Leahu, M. L. Grilli, A. Sytchkova, C. Sibilia, R. L. Voti, *Phys. Status Solidi C* **2016**, *13*, 998.
[20] P. Tockhorn, J. Sutter, R. Colom, L. Kegelmann, A. Al-Ashouri, M. Roß, K. Jäger, T. Unold, S. Burger, S. Albrecht, C. Becker, *ACS Photonics* **2020**, *7*, 2589.
[21] P. Tockhorn, J. Sutter, A. Cruz, P. Wagner, K. Jäger, D. Yoo, F. Lang, M. Grischek, B. Li, J. Li, O. Shargaieva, E. Unger, A. Al-Ashouri, E. Köhnen, M. Stolterfoht, D. Neher, R. Schlatmann, B. Rech, B. Stannowski, S. Albrecht, C. Becker, *Nat. Nanotechnol.* **2022**, *17*, 1214.
[22] Z. Ying, X. Guo, H. Du, X. Li, M. Zhang, Y. Zeng, X. Yang, J. Ye, *ACS Energy Lett.* **2024**, *9*, 4018.
[23] J. Bonse, *Nanomaterials* **2020**, *10*, 1950.
[24] A. Rank, V. Lang, A. F. Lasagni, *Adv. Eng. Mater.* **2017**, *19*, 1700201.
[25] MatWeb materials database, https://matweb.com/, website (accessed: February 2024).
[26] Q. Lin, L. Lu, M. M. Tavakoli, C. Zhang, G. C. Lui, Z. Chen, X. Chen, L. Tang, D. Zhang, Y. Lin, P. Chang, D. Li, Z. Fan, *Nano Energy* **2016**, *22*, 539.
[27] Y. Zhu, L. Shu, S. Poddar, Q. Zhang, Z. Chen, Y. Ding, Z. Long, S. Ma, B. Ren, X. Qiu, Z. Fan, *Nano Lett.* **2022**, *22*, 9586.
[28] K. Jäger, C. Barth, M. Hammerschmidt, S. Herrmann, S. Burger, F. Schmidt, C. Becker, *Opt. Express* **2016**, *24*, A569.
[29] M. Soldera, Q. Wang, F. Soldera, V. Lang, A. Abate, A. F. Lasagni, *Adv. Eng. Mater.* **2020**, *22*, 1901217.